On computing first and second order derivative spectra

Indrajit G. Roy *

Spaceage Geoconsulting, PO Box 6154, Conder, ACT 2906, Australia

A B S T R A C T

Enhancing resolution in spectral response and an ability to differentiate spectral mixing in delineating the *endmembers* from the spectral response are central to the spectral data analysis. First and higher order derivatives analysis of absorbance and reflectance spectral data is commonly used techniques in differentiating the spectral mixing. But high sensitivity of derivative to the noise in data is a major problem in the robust estimation of derivative of spectral data. An algorithm of robust estimation of first and second order derivative spectra from evenly spaced noisy normal spectral data is proposed. The algorithm is formalized in the framework of an inverse problem, where based on the fundamental theorem of calculus a matrix equation is formed using a Volterra type integral equation of first kind. A regularization technique, where the balancing principle is used in selecting *a posteriori* optimal regularization parameter is designed to solve the inverse problem for robust estimation of first order derivative spectra. The higher order derivative spectra are obtained while using the algorithm in sequel. The algorithm is tested successfully with synthetically generated spectral data contaminated with additive white Gaussian noise, and also with real absorbance and reflectance spectral data for fresh and sea water respectively.

© 2015 Elsevier Inc. All rights reserved.

1. Introduction

Enhanced resolution without bringing noise artifact in spectroscopic technique is an essential step in spectroscopic analysis of a complex substance. This is because spectral contributions by the components within a substance under investigation often overlap in the measured spectral band making it difficult to identify and separate their contributions individually. In fact, such issue has been well recognized over many years and was attempted to resolve as early as middle of twentieth century [1–4]. There is a record of various approaches over more than six decades to enhance resolution, chiefly either through Fourier based self deconvolution [5,6] or by incorporating derivative of the spectra; in that derivative method has taken a significant place in today's spectroscopy technique.

Initial attempt in incorporating derivative on the measured spectra were restricted with the hardware by designing either appropriate optical set up, such as scanning spectrophotometer of various make or through appropriate electronic circuitry. A detailed discussion on hardware based method is available in [7]. However, derivative spectroscopy through hardware implementation has limitations, such as 1) restricted limit on the order of derivative in the measured spectra, 2) increasing difficulty in noise control with the increase in order of derivative and 3) a shift in amplitude and wavelength of the derivatives due to variation in the scan speed for optical scan based technique.

---

* Tel.: +61 2 6294 2510.
  E-mail address: spaceage.geocon@gmail.com.

Computational approach, on the other hand, is highly flexible. The noise reduction in the measurement becomes greatly simplified. With today's technology of high speed computing and flexibility, one can have, almost a real time, derivative spectra from the measurement of normal spectra. Despite such advantage a robust, reliable computationally efficient method of derivative estimation, especially of large and noisy dataset remains elusive. Even today the difference method of computing derivative is most popular and is widely used technique, as it is found to be a simplest means of computing derivative from evenly spaced tabulated data using Excel™ spreadsheet. But such simplicity in computing comes with a price of compromising fidelity by increasing the effect of noise in data. More densely (i.e. reduction in data interval) the spectral data is measured the effect of noise in data becomes more pronounced in computed derivative using a difference scheme. Unreliability even grows further with the increase in noise magnitude and the order of derivatives. With a common belief, the reduction in reliability in estimated derivative via difference method is somewhat counter intuitive, as from the first principle of differential calculus computational accuracy should increase with decreasing data interval as long as the denominator remains non-zero or does not attain the underflow limit of a computer.

The measured data, however, contain random noise in general, and such noise has dominant effect on the high frequency part of the measurements. Since, a difference scheme which is essentially based on polynomial interpolation acquires the attribute of low pass filtering. Larger the data spacing higher is the filtering effect. An optimal data spacing which is most sought after is, however, hard to achieve. It was demonstrated in [8] that for the noise level δ in data a minimal error of magnitude $2\sqrt{\delta}$ can be attained for a second order central difference scheme, if the denominator δx ($= l\Delta$, with l an integer) approximates closely to δ. It then turns out that one needs to discard some data samples from a closely sampled dataset to gain the desired accuracy within a predetermined noise level. Such strategy is, however, not encouraging as A) one is often left with a little option of pre-selecting the data spacing (or the sampling rate) and B) the choice of larger δx leads to a lose of information from a highly sampled dataset.

Other popular approach, mostly embraced by geophysics community, is Fourier method in computing derivative of evenly distributed data. The motivation in adopting the technique is chiefly due to computational efficiency while handling a large data through Fast Fourier transform (FFT) algorithm, although additional steps involved, such as trend removal, appropriate windowing and zero padding makes the method somewhat tedious. Despite all, the most worrying aspect is that the method is sensitive to additive white Gaussian noise (AWGN). Higher the order of derivative, more susceptible it becomes with the noise in data. Therefore, derivative computation without noise removal using an appropriate filter cannot be an option. The requirement of filtering to tackle the noise issue (especially with AWGN) makes Savitzky–Golay (SG) moving polynomial method [9,10] an alternative approach for derivative spectroscopy. The performance of SG method, however, depends on the size of the window and the degree of polynomial chosen. Larger window would cause a high level of smoothness; conversely significantly small window size may not be able to attain the desired level of noise reduction. Another popular approach is polynomial fitting method [11,12] where the measured dataset is fitted with an appropriate polynomial globally and then derivative is computed on the polynomial. The limitation of such method is to find an optimal order of polynomial. Often, selecting a higher order polynomial brings in computational instability due to Runge effect [12].

On the other hand, the recent trend is towards regularization technique which would provide the much desired stable solution in derivative estimation while remaining not too expensive computationally. There are various strategies in estimating derivative using regularization technique. For example, in [13] a regularized spline technique was used in estimating derivative of discrete unevenly spaced dataset. Other approaches are: 1) use of integral equation, such as Fredholm integral equation of first kind [35], Volterra integral equation [14,15] together with Tikhonov regularization technique, 2) use of integral equation and total variation regularization in estimating derivative from noisy data set [16], 3) finite difference technique with optimally chosen step size [36], use of dynamical system method [37].

We propose a novel technique which is sufficiently robust and computationally efficient in estimating derivative of noisy spectral data. We formalize the derivative estimation problem as an inverse problem. Using the fundamental theorem of calculus a matrix operator equation is designed from a Volterra type integral equation of first kind. The inverse problem is solved in the framework of a constrained optimization via regularization where an optimal value of regularization parameter is determined using '*balancing principle*'. We demonstrate robustness and efficiency of the proposed algorithm using numerical experiments on synthetically generated data which are contaminated with AWGN. We then use it in analyzing absorption and reflectance spectra within the visible range to study phytoplankton and other dissolved organic matters in pure water [32] and sea water [33] respectively.

The paper is organized as followed: In Section 2 we give a brief discussion on the theoretical background for our proposed algorithm. In Section 3 we discuss about the results obtained from the numerical experiments conducted on synthetically generated spectral data contaminated with AWGN. We also demonstrate with illustrations how conventional Fourier transform based method and central difference scheme in derivative computation fail when data contain AWGN even in a mild level. We then applied our method in estimating first and second order derivatives of absorbance and reflectance spectral data within the visible range to study the phytoplankton and other dissolve organic matters in both fresh water lake and sea water to demonstrate the applicability of the algorithm. The paper then concludes with a brief conclusion.

2. Formulation

Suppose that $f(x)$ is a continuously differentiable, smooth function within an interval $[a, b]$ for which $u(x)$, a continuous function, is the first derivative. Actually, we deal with evenly sampled discrete 1D data, such as $\{f_1, f_2, \ldots, f_N\}$ defined over

a regular grid with a grid interval Δ. From the first fundamental theorem of calculus a smooth continuously differentiable function $f(x)$ and its first order derivative $u(x)$ is related as

$$f(x) = f(a) + \int_a^x \partial_s f(s)ds = f(a) + \int_a^x u(s)ds \quad \text{for all } x \in [a,b] \tag{2.1}$$

The extra term $f(a)$ corresponds to dc shift. If the spectral data are baseline corrected then $f(a) = 0$. Further, using second fundamental theorem of calculus the function $u(x)$ is integrable under Riemannian sense, which means that if the interval be partitioned into subintervals so that two adjacent subintervals have common end points then the partial sum of the product of length of the subinterval with the value of function at any point within the subinterval approximates closely the value of integral as the 'mesh of partition' approaches zero. The 'mesh of partition' is defined as the maximum length of the subintervals. This allows one to implement a quadrature rule. There are various quadrature rules, but the simplest one for a definite integral $J = \int_a^b u(x)dx$ is the rectangular rule [17], and is written as

$$J = \int_a^b u(x)dx \approx \Delta\big[u(\hat{x}_1) + u(\hat{x}_2) + \cdots + u(\hat{x}_N)\big], \tag{2.2}$$

where the interval $[a,b]$ is partitioned into N equally spaced subintervals of length $\Delta = (b-a)/N$. The quadrature rule (2.2) indicates summation of N-rectangles of width Δ. But N equally spaced subintervals makes $N+1$ grid points written as $a = \hat{x}_1 < \hat{x}_2 < \ldots < \hat{x}_{N+1} = b$. However, if $\mathbf{f} = (f_1, f_2, \ldots, f_N)^T$ is the vector of evenly spaced data values of the regular function corresponding to each rectangle, then it is possible to write the following matrix equation using Eqs. (2.1) and (2.2)

$$\mathbf{Au} = \mathbf{f}, \tag{2.3}$$

where $\mathbf{u}$ is the vector of first order derivative of the function corresponding to the vector of sample values $\mathbf{f} = (f_1, f_2, \ldots, f_N)^T$ and the matrix $\mathbf{A}$ which can be termed as design matrix is written as

$$\mathbf{A} = \begin{pmatrix} \Delta & 0 & 0 & 0 & 0 & 0 \\ \Delta & \Delta & 0 & 0 & 0 & 0 \\ \Delta & \Delta & \Delta & 0 & 0 & 0 \\ \ddots & \ddots & \ddots & \ddots & \ddots & \ddots \\ \Delta & \Delta & \Delta & \cdots & \Delta & 0 \\ \Delta & \Delta & \Delta & \cdots & \Delta & \Delta \end{pmatrix}_{N \times N}, \tag{2.4}$$

Other closely related to the rectangular rule is the trapezoidal rule which according to [17] is written as.

$$J = \int_a^b u(x)dx \approx \hat{\Delta}\Big[\frac{1}{2}u(\hat{x}_1) + u(\hat{x}_2) + \cdots + u(\hat{x}_N) + \frac{1}{2}u(\hat{x}_N)\Big], \tag{2.5}$$

where the interval $[a,b]$ is partitioned into $N-1$ equally spaced subintervals of length $\hat{\Delta} = (b-a)/(N-1)$, such that $a = \hat{x}_1 < \hat{x}_2 < \ldots < \hat{x}_N = b$. If $\mathbf{f} = (f_1, f_2, \ldots, f_N)^T$ is the vector of evenly spaced sample values of the regular function then it is possible to write the matrix equation as in (2.3), where the designed matrix $\mathbf{A}$ is written as

$$\mathbf{A} = \begin{pmatrix} \frac{1}{2}\hat{\Delta} & 0 & 0 & \cdots & 0 & 0 \\ \frac{1}{2}\hat{\Delta} & \frac{1}{2}\hat{\Delta} & 0 & \cdots & 0 & 0 \\ \frac{1}{2}\hat{\Delta} & \hat{\Delta} & \frac{1}{2}\hat{\Delta} & \cdots & 0 & 0 \\ \ddots & \ddots & \ddots & \ddots & \ddots & \ddots \\ \frac{1}{2}\hat{\Delta} & \hat{\Delta} & \hat{\Delta} & \cdots & \frac{1}{2}\hat{\Delta} & 0 \\ \frac{1}{2}\hat{\Delta} & \hat{\Delta} & \hat{\Delta} & \cdots & \hat{\Delta} & \frac{1}{2}\hat{\Delta} \end{pmatrix}_{N \times N} \tag{2.6}$$

Often it is perceived, in general, that between rectangular and trapezoidal quadrature rule the trapezoidal rule provides more accurate results than the former, which is unfortunately misleading. It is possible to demonstrate (which is not included in the text) that the converse is the true. Further, we will demonstrate in the section on numerical experiment that considering the design matrix $\mathbf{A}$ as in Eq. (2.6) is rather disadvantageous.

For a set of N discrete data values the matrix $\mathbf{A}$ is a lower triangular matrix of order $N \times N$, which suggests that derivative of the data can be obtained from Eq. (2.3) by simply adopting to the method of back substitution. Such a simplistic situation, although much wanted, does not provide desired results often in all practical purposes. Firstly, solution depends strongly on the condition of the matrix $\mathbf{A}$ that steadily becomes unfavorable as the dimension of the system increases with decreasing value of Δ. Secondly, the reliability in derivative estimation decreases steadily with an increase of noise level; even with a moderate noise level the system renders unacceptable results. Therefore, instead of inverting the matrix $\mathbf{A}$ directly it is necessary to reformulate the problem while considering that the discrete dataset is indeed contaminated with noise having a noise level δ, where the noise level δ is denoted in terms of root mean square amplitude of the additive noise.

2.1. Regularization

At the outset we recognize that the measured data indeed contain noise. The noise contaminated dataset is denoted as $\mathbf{f}^\delta$. We want our estimated derivative should reflect least on noise in data. In other words, the variation of the estimated derivative globally should be the least. A measure of such variation is the first order differential on $\mathbf{u}$, which can be written as

$$\hat{\mathbf{D}}\mathbf{u} = \Delta^{-1} \begin{bmatrix} -1 & 1 & 0 & 0 & \cdots & 0 \\ 0 & -1 & 1 & 0 & \cdots & 0 \\ \vdots & \vdots & \ddots & \ddots & \ddots & \vdots \\ \vdots & \vdots & \cdots & -1 & 1 & 0 \\ 0 & 0 & \cdots & 0 & -1 & 1 \end{bmatrix}_{(N-1)\times N} \begin{bmatrix} u_1 \\ u_2 \\ \vdots \\ u_{N-1} \\ u_N \end{bmatrix}_{N\times 1} \tag{2.7}$$

Our reformulation is based on imposing a constraint, such as *minimize* $\|\hat{\mathbf{D}}\mathbf{u}\|_2^2$ *such that* $\|\mathbf{A}\mathbf{u} - \mathbf{f}^\delta\|_2^2 < c\delta^2$, where $c > 1$ is an arbitrary constant. In other words, minimize the variation in estimated derivative as a solution, while keeping a track that the response computed from such solution approximate measurements within the limit of noise level. It can be said that a minimizer $\mathbf{u}$ can be obtained as

$$\mathbf{u}_\beta^\delta = \min_{\mathbf{u}} \Phi(\mathbf{u}) \triangleq \arg\min_{\mathbf{u}} \left[\frac{1}{2}\|\hat{\mathbf{D}}\mathbf{u}\|_2^2 + \frac{\beta}{2}\|\mathbf{A}\mathbf{u} - \mathbf{f}^\delta\|_2^2 \right], \tag{2.8}$$

where $\Phi(\mathbf{u})$ is a composite function. On implementing the condition of vanishing gradient of Φ we get Euler–Lagrange equation as

$$\left(\mathbf{A}^T\mathbf{A} + \alpha\hat{\mathbf{D}}^T\hat{\mathbf{D}}\right)\mathbf{u} - \mathbf{A}^T\mathbf{f}^\delta = 0, \tag{2.9}$$

where $\alpha = \beta^{-1}$ is suitably chosen scalar quantity satisfying an obvious constraint $\alpha > 0$. The parameter α is widely known as regularization parameter. Note that the above equation (2.9) is essentially the outcome of well known Tikhonov regularization [18]; however, many author prefers to call it Tikhonov regularization if the operator $\hat{\mathbf{D}} = \mathbf{I}$. The performance of Eq. (2.9) in estimating solution $\mathbf{u}$ depends largely on the selection of the regularization parameter α, as the value of α weighs as a penalty in upholding the constraint while minimizing the smoothing functional Φ. A substantially small value of α may make the estimated derivative more wiggly for not providing enough penalty in violating the constraints; a very large value of α, on the other hand, would make solution too smooth to be acceptable. To this end, we must admit that if the data contain no noise at all then the value of α should either be zero or at least becomes very small. But in many practical situations, such as 1) the uncertainty in measurement, 2) the limitation due to algorithmic precision and 3) the intrinsic property of ill-posedness of the operator $\mathbf{A}$ do not allow for vanishing α value. A suitable value of α should make a balance between the fidelity $\|\mathbf{A}\mathbf{u} - \mathbf{f}^\delta\|_2^2$ and the penalty terms $\|\hat{\mathbf{D}}\mathbf{u}\|_2^2$, and hence it seems appropriate to formulate a method based on such principle, also known as method of 'balancing principle' [20,21]. To this end, we note that there are various strategies of determining regularization parameter, such as L-curve technique [19], modified L-curve [22–24], generalized cross validation [25,15], discrepancy principle [26], modified discrepancy principle [27–29], and every strategy has some relative merit and demerit as well. The greatest strength of 'balancing principle' in selecting the value of regularization parameter α *a posteriori* is due to following attributes: 1) it is physically intuitive as it invokes a balance between approximation error and the computational stability and 2) its independence on the knowledge of noise level in data. However, we also note that there is no possibility to determine a unique value of α.

There exist three possible forms of solutions to the linear system (Eq. (2.3)). First category corresponds to the true solution $\mathbf{u}^\dagger$ when we know data exactly, which should require no penalty ($\alpha = 0$) at all. Second category corresponds to a general situation $\mathbf{u}_\alpha^\delta$, where data contaminated with noise is available for which we get a solution that is based on satisfying constraint of smoothness, and therefore it involves a penalty ($\alpha \neq 0$). The third category corresponds to a solution $\mathbf{u}_\alpha$ which is a best estimation to the true solution when data contain no noise. The third category of solution is actually a generalized representation of a solution obtained through an optimization algorithm under the condition that the data is free from noise. In the following we write the smoothing functional by omitting the multiplying factor 1/2 as

$$\mathbf{u}_\alpha^\delta = \arg\min_{\mathbf{u}}\left\{\Phi(\mathbf{u}, \alpha)\right\} \quad \text{with } \Phi(\mathbf{u}, \alpha) = \|\mathbf{A}\mathbf{u} - \mathbf{f}^\delta\|_2^2 + \alpha\|\hat{\mathbf{D}}\mathbf{u}\|_2^2 \doteq \varphi(\mathbf{u}) + \alpha\psi(\mathbf{u}), \tag{2.10}$$

where $\mathbf{u}_\alpha^\delta$, a minimizer, corresponds to a solution when data contain noise with noise level δ, the functional φ and ψ are non-negative and are termed as fidelity and penalty terms respectively. It is reasonable to consider that a minimizer $\mathbf{u}_\alpha^\delta$ corresponding to the regularization parameter α belongs to a set of minimizers $\mathcal{U}^\alpha$. We are, however, interested in selecting a particular minimizer $\mathbf{u}_{\alpha_*}^\delta$ which corresponds to a regularization parameter α_*, whose value should satisfy a certain optimality condition imposed. The optimality condition is, however, based on some physical extension. For example, with the popular Morozov's *discrepancy principle* [26] the optimality condition is assigned with the fidelity term, such that an optimal α_* should satisfy the condition $\varphi(\mathbf{u}_{\alpha_*}^\delta) = \delta^2$, which implies that a regularization parameter be so chosen that the solution based on it would maintain fidelity within the noise variance in measurements. In other occasion, such as with

an L-curve technique or its variant [22,23] the optimality condition is assigned jointly on both the functionals related to fidelity and penalty terms; in that an optimum regularization parameter α_* makes a trade-off between the fidelity and the penalty terms, whereby it becomes a minimizer to a suitably defined function $\Psi(\alpha) = \varphi(\mathbf{u}_\alpha^\delta) \cdot \psi^\eta(\mathbf{u}_\alpha^\delta)$, with $0 < \eta \le 1$. We, however, consider the optimality condition based on 'balancing principle' as proposed in [20]. The principle suggests that a regularization parameter α is chosen in such a manner that the solution based on it would allow the contribution due to fidelity term being balanced by the contribution due to penalty term. Accordingly, it is written as

$$\varphi(\mathbf{u}_\alpha^\delta) = \gamma \alpha \psi(\mathbf{u}_\alpha^\delta) \quad \text{with } \gamma > 0, \text{ for } \mathbf{u}_\alpha^\delta \in \mathcal{U}^\alpha \tag{2.11}$$

Following [20] we define a function $\Theta(\alpha) = \inf_{\mathbf{u}} \Phi(\mathbf{u}, \alpha)$ which is monotonic, concave and almost everywhere differentiable (an interested reader may find the proof of this statement in Theorem 2.1 of [20]). Using Eq. (2.10) it is trivial to establish the following expression

$$\frac{d\Theta(\alpha)}{d\alpha} = \psi(\mathbf{u}_\alpha^\delta), \quad \text{for } \mathbf{u}_\alpha^\delta \in \mathcal{U}^\alpha \tag{2.12}$$

Clearly, the derivative of the function $\Theta(\alpha)$ is non-negative. Further, we define another function $\Omega_\nu(\alpha)$ as

$$\Omega_\nu(\alpha) = \frac{\Theta^{\nu+2}(\alpha)}{\alpha^2}, \tag{2.13}$$

where $0 < \nu < 1$ is a free parameter whose value may be suitably chosen. The major motivation in defining the new function $\Omega_\nu(\alpha)$ is that it would facilitate in selecting an appropriate value of α for which the optimality condition (2.11) holds. Let us examine the property of the function $\Omega_\nu(\alpha)$. Since, $\Theta(\alpha)$ is monotonically increasing and concave then the function $\Theta^{\nu+2}(\alpha)$ also possesses the same properties. Further, it is safe to assert that the function α^{-2} is concave as its inverse is monotonic and convex. Therefore, the function $\Omega_\nu(\alpha)$ is also concave, and hence there exists a minimizer of the function $\Omega_\nu(\alpha)$. It then follows from upholding the optimality condition

$$\frac{d\Omega_\nu(\alpha)}{d\alpha} = \frac{\Theta^{\nu+1}(\alpha)}{\alpha^2} \cdot \frac{[(\nu+2)\alpha \frac{d\Theta(\alpha)}{d\alpha} - \Theta(\alpha)]}{\alpha} = 0 \tag{2.14}$$

With a little algebraic manipulation from Eq. (2.14) we can write

$$\alpha = \frac{1}{(\nu+1)} \cdot \frac{\varphi(\mathbf{u}_\alpha^\delta)}{\psi(\mathbf{u}_\alpha^\delta)} \tag{2.15}$$

Note that the striking similarity between Eqs. (2.15) and (2.11), where the factor γ is replaced by $(\nu+1)^{-1}$. It is also important to note that with the 'balancing principle', the value of α is not dependent explicitly on the noise level in data. Nevertheless, experimental data contain noise in general, and it is essential to ensure that the regularized solution $\mathbf{u}_{\alpha_*}^\delta$, where α_* is an optimal value of regularization parameter, should approximate closely the true solution $\mathbf{u}^\dagger$ (which is often not known in general), or at least be bounded within a closed region surrounding the true solution. This requires additional condition, known as source condition, which describes a kind of smoothness constraint on the true solution, to be satisfied. The rationale behind such assertion is that the algorithm for regularized solution must ensure an improved rate of convergence. The source condition (in general) for a linear operator equation, such as Eq. (2.3) demands that the true solution $\mathbf{u}^\dagger$ of it must lie in the range of the adjoint of the operator $\mathbf{A}$, or in other words, $\mathbf{u}^\dagger = \mathbf{A}^T \mathbf{f}^\dagger$, where $\mathbf{f}^\dagger$ is ideally the data vector for which the true solution exists, so that the regularized solution converges in a best possible manner. The above source condition is of low order, too stringent and is difficult to satisfy in many occasions [38]. A higher order source condition is a Hölder type source condition which states $\mathbf{u}^\dagger = (\mathbf{A}^T \mathbf{A})^\mu \mathbf{w}$, $0 < \mu \le 1$, where $\mathbf{w}$ is a vector which belongs to the same space as the original solution. It is demonstrated in [21], under Hölder type source condition, and in [30] under newly defined optimization based source condition the approximation error in the regularized solution corresponding to regularization parameter α_* determined via 'balancing principle' is bounded, and it can be written as

$$\|\mathbf{u}^\dagger - \mathbf{u}_{\alpha_*}^\delta\| \le c \max\{\delta_*, \delta\}^{\frac{2t}{2t+1}}, \quad \text{with } t \in (0, 1] \text{ and } c > 0 \tag{2.16}$$

where $\delta_* = \|\mathbf{A}\mathbf{u}_{\alpha_*}^\delta - \mathbf{f}^\delta\|$ is the residual.

We propose in the following an iterative algorithm where the stopping criterion for the iterative algorithm to cease iteration is based on satisfying the discrepancy measure

$$\|\mathbf{A}\mathbf{u}_{\alpha_*}^\delta - \mathbf{f}^\delta\| = \tau \delta, \quad \text{with } \tau > 1 \tag{2.17}$$

We give a pseudo code description of the algorithm in the following:

Algorithm.

Input: Array of (x, y) data and an estimate of noise level δ
Generate: $\mathbf{A}$ and $\mathbf{D}$ matrices
Set: $k = 0$,
Choose: $\alpha_0 = \delta^{\frac{2}{3}}$
Do while $\|\mathbf{Au}_{\alpha_k}^{\delta} - \mathbf{f}^{\delta}\| > \tau\delta$
        Compute: $\mathbf{u}_{\alpha_k}^{\delta} = (\mathbf{A}^T\mathbf{A} + \alpha_k\hat{\mathbf{D}}^T\hat{\mathbf{D}})^{-1}\mathbf{A}^T\mathbf{f}^{\delta}$
        Increment: $k = k + 1$
        Compute: $\alpha_k = (\nu + 1)^{-1} \cdot \frac{\|\mathbf{Au}_{\alpha}^{\delta} - \mathbf{f}^{\delta}\|_2^2}{\|\hat{\mathbf{D}}\mathbf{u}_{\alpha}^{\delta}\|_2^2}$
End Do

Note that on exiting the iterative loop while satisfying the condition $\|\mathbf{Au}_{\alpha_*}^{\delta} - \mathbf{f}^{\delta}\| > \tau\delta$ the final value of α_k together with $\mathbf{u}_{\alpha_k}^{\delta}$ is ultimately chosen.

2.2. Noise level estimation

The proposed algorithm actually needs an assessment of noise in data, although it is not required explicitly as an input in determining the regularization parameter α. Estimating the noise level in the spectral data from a single set of measurements is, however, a non-trivial task. We consider a simple strategy in estimating an error level in data. We maintain the general view that the true signal (here the spectral data) is sufficiently smooth, whereas the measured one is noise contaminated and hence it is wildly varying due to the presence of Gaussian distributed random noise. We consider a median filter, more specifically an iterative median filter to get a smoothed or filtered output. The rationale in considering median filter are: 1) it provides a robust estimation especially with additive Gaussian noise and is best known for preserving the shape of the signal and 2) for 1D signal it is computationally simple and efficient. Shape preserving, edge restoration while removing noises (especially short random pulses) are important aspects in the realm of image processing where a wide variant of median filter are designed to address those issues. However, we are not to be much worried about those in the present context as our need is only to get an estimate of the data error for 1D spectral data. The median filtering approach that we propose is given with pseudo codes in the following:

Choose: a filter window of appropriate length;
Set: the threshold value of ε, a small number;
Set: $\mathbf{f}^{old} = \mathbf{f}^{\delta}$
Compute: $\mathbf{f}^{new} = median\,filter(\mathbf{f}^{old})$
Do until: mean absolute error $\sum_{i=1}^{N}|f_i^{old} - f_i^{new}|/N \leq \varepsilon$
        Set: $\mathbf{f}^{old} = \mathbf{f}^{new}$
        Compute: $\mathbf{f}^{new} = median\,filter(\mathbf{f}^{old})$
End Do

The proposed strategy quickly attains root of the median filter. Most importantly, unlike conventional single pass median filter, the method works well even with a short filter window length. In selecting the filter window we select the portion of the curve where the curve reflects least variation; in other words, a minimum slope. The selection of threshold value ε is somewhat arbitrary; however, we have chosen it as 10^{-3} after conducting numerical experiment with some trial values of ε. We observe that lowering threshold value further causes only a marginal improvement in the estimation of noise level δ, which is estimated as $\delta \approx \|f^{\delta} - f^{new}\|_2$.

3. Numerical experiment

3.1. Synthetic spectral data

We consider Gaussian function as a synthetic prototype of a spectra, as also used in [31] for numerical experiment. Suppose that a synthetically generated spectra is a combination of two Gaussians written as

$$A = A_{m1}\exp\left[-\left(\frac{\lambda - \lambda_{\omega 1}}{\sigma_1}\right)^2\right] + A_{m2}\exp\left[-\left(\frac{\lambda - \lambda_{\omega 2}}{\sigma_2}\right)^2\right], \tag{3.1}$$

where A_{m1} and A_{m2} are amplitudes of two overlapping spectra, $\lambda_{\omega 1}$ and $\lambda_{\omega 2}$ are the wavelengths of the Gaussians where the spectral bands attain respective maxima, and σ_1 and σ_2 are the parameters related to *full width at half maximum* (FWHM) parameters $\omega 1$ and $\omega 2$ of the two Gaussian spectra as
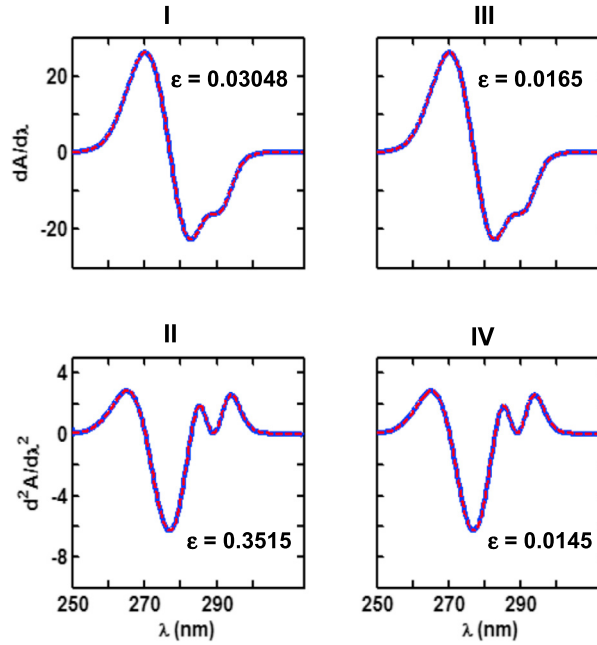
Fig. 1. Panels (I) and (II) estimated first and second order derivative spectra (solid blue lines) from noise-free synthetically generated spectral data (using Eq. (3.1)) via Fourier transform based technique respectively. Panels (III) and (IV) are same as panels (I) and (II) but estimation is obtained using central difference technique. The computed true value (red colored stippled line) is overlaid on it. The value of ε in each panel is residual error. The sampling interval of discrete data set is 0.25 nm. (For interpretation of the references to color in this figure legend, the reader is referred to the web version of this article.)

$$\sigma_1 = \frac{\omega1}{2\sqrt{\ln 2}} \quad \text{and} \quad \sigma_2 = \frac{\omega2}{2\sqrt{\ln 2}}$$

The analytical expressions of first and second order derivatives are given as

$$\frac{\partial A}{\partial \lambda} = -\frac{2}{\sigma_1} A_{m1}\left(\frac{\lambda - \lambda_{\omega1}}{\sigma_1}\right) \exp\left[-\left(\frac{\lambda - \lambda_{\omega1}}{\sigma_1}\right)^2\right] - \frac{2}{\sigma_2} A_{m2}\left(\frac{\lambda - \lambda_{\omega2}}{\sigma_2}\right) \exp\left[-\left(\frac{\lambda - \lambda_{\omega2}}{\sigma_2}\right)^2\right] \tag{3.2}$$

and

$$\frac{\partial^2 A}{\partial \lambda^2} = \frac{2A_{m1}}{\sigma_1^2}\left[2\left(\frac{\lambda - \lambda_{\omega1}}{\sigma_1}\right)^2 - 1\right] \exp\left[-\left(\frac{\lambda - \lambda_{\omega1}}{\sigma_1}\right)^2\right] + \frac{2A_{m2}}{\sigma_2^2}\left[2\left(\frac{\lambda - \lambda_{\omega2}}{\sigma_2}\right)^2 - 1\right] \exp\left[-\left(\frac{\lambda - \lambda_{\omega2}}{\sigma_2}\right)^2\right] \tag{3.3}$$

We then select same parameter values as also used in [31], such as

$$A_{m1} = 0.293, \quad \omega1 = 16.013 \text{ nm}, \quad \lambda_{m1} = 277 \text{ nm},$$

$$A_{m2} = 0.030, \quad \omega2 = 7.771 \text{ nm}, \quad \lambda_{m2} = 289 \text{ nm},$$

and then generate the spectral response for wavelengths λ ranging from 250–300 nm with a sampling interval $\Delta\lambda = 0.25$ nm. The proposed algorithm actually computes the first order derivative. We therefore consider a sequential approach to compute derivatives higher than the first order as shown below:

Derivative 0*th order* $\rightarrow$ *Derivative* 1*st order* $\rightarrow$ *Derivative* 2*nd order*

This means, same algorithm will be used successively to determine higher order derivatives. Such strategy has following advantages: 1) by sequential approach one can compute derivatives in any arbitrary order and 2) one can monitor noise sensitivity in the computed derivative and decide whether to progress further.

Although in the proposed algorithm the knowledge of noise level is not highly essential in determining the regularization parameter, the noise level in data is nonetheless a necessary input for the algorithm to enforce stopping criterion which is based on discrepancy principle. The discrepancy principle states that the estimated residual error level δ_* should lie within a close neighborhood of the noise level δ. The size of the neighborhood is determined through the value of the multiplicative factor τ. We consider the value of τ as 1.01 in our experiment. The value of ν (Eq. (2.14)) is kept as 0.25. The algorithm starts with an initial value of $\alpha \sim \delta^{\frac{2}{3}}$ which modifies iteratively using Eq. (2.14).

We first demonstrate the performance of conventional techniques, such as the difference scheme and the Fourier transform based derivative computation. We may call those techniques as direct method in oppose to the proposed technique.
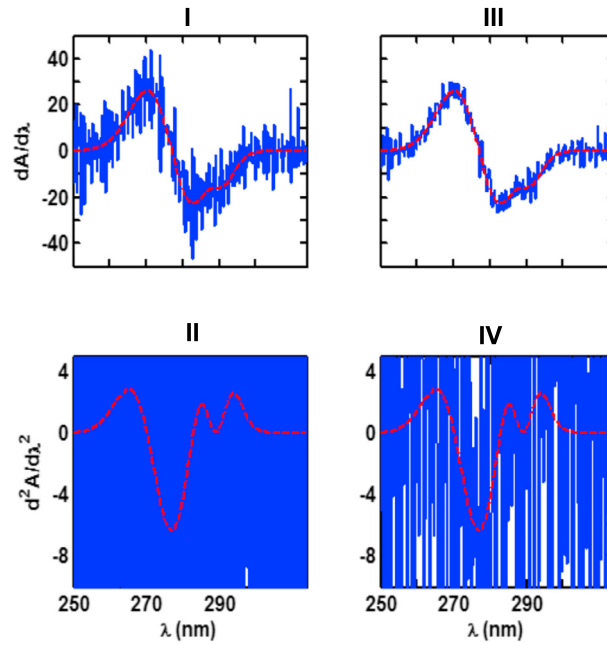
Fig. 2. The subplots in panels (I)–(IV) are same as Fig. 1, except that the discrete data contain AWGN with SNR 40 dB. (For interpretation of the references to color in this figure, the reader is referred to the web version of this article.)

The results of those schemes for noise free data are presented in Fig. 1. For the sake of visual ease in comparing we put all figures in one panel using subplots. The first column of Fig. 1 (marked with I, II) contains first and second orders derivative spectra computed using Fourier transform based technique (blue colored thick solid line) overlaid with synthetically generated (red colored stippled line) of first and second order derivative spectra using Eqs. (3.2) and (3.3) respectively. On the other hand, the second column of Fig. 1 (marked with III and IV) contains first and second orders derivative spectra computed using central difference scheme (blue colored thick solid line) overlaid with synthetically generated responses (red colored stippled line) of first and second order derivative spectra. The value of ε within each subplot is the error measure defined as maximum of the absolute residuals between the estimated derivatives with the synthetic one. Note that in terms of visual comparison both the Fourier transform based technique and the central difference scheme on noise free data provides reasonably good results; however, difference scheme is more robust compared to Fourier transform based technique especially in estimating second order derivative spectra. We then contaminated synthetically generated data with AWGN of signal-to-noise ratio (SNR) 40 dB and carried out numerical experiment using Fourier transform and central difference scheme. The results are presented in Fig. 2. As in earlier the first column of Fig. 2 (marked with I, II) contains first and second orders derivative spectra computed using Fourier transform based technique (blue colored thick solid line) overlaid with synthetically generated (red colored stippled line) of first and second order derivative spectra respectively while the second column (marked with III and IV) contains first and second orders derivative spectra computed using central difference scheme (blue colored thick solid line) overlaid with synthetically generated responses (red colored stippled line) of first and second order derivative spectra. The performance of both the technique is unacceptable, although performance wise Fourier transform based technique is the worst. This is conceivable, as without any pre-processing of noisy data with a filter the energy of high frequency noise component increases with a multiplicative order of frequency in case of Fourier transform based technique. However, the difference scheme is marginally better off, as it imposes a kind of low pass filtering effect. Larger is the grid interval higher becomes the filtering effect. To demonstrate it we generated synthetic data with an interval of 1 nm, contaminated the data with AWGN of SNR 40 dB and then used it for numerical experiment. The results are presented in Fig. 3 with subplots and the subplots are arranged in the same fashion as it is in Fig. 2. Clearly, the results due to difference scheme outperform those due to Fourier transform method, and there is a substantial improvement over the earlier results.

We then conducted numerical experiment with the proposed scheme on synthetically generated normal spectral data (using Eq. (3.1)) contaminated with AWGN with three different SNR levels such as 40, 30 and 20 dB respectively. However, for the sake of maintaining brevity we will cite examples corresponding to the extreme ends of noise levels only. We conducted numerical experiment using both the designed matrix (Eqs. (2.4) and (2.6)). We will discuss in the following numerical implications in selecting a suitable designed matrix.

In order to maintain an ease in comparing results we keep results due to normal, first and second order derivative spectra as subplots in the same panel of a figure, marked with I, II and III respectively. Fig. 4 contains results of numerical experiments on synthetic data contaminated with AWGN of SNR 40 dB where the design matrix **A** based on rectangular
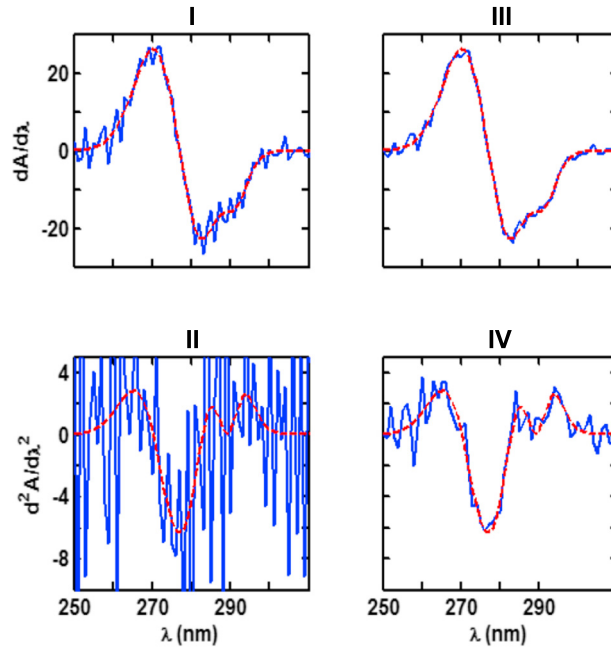
Fig. 3. The subplots in panels (I)–(IV) are same as Fig. 1, but the discrete data set has the sampling interval 1 nm and it contains AWGN with SNR 40 dB. (For interpretation of the colors in this figure, the reader is referred to the web version of this article.)
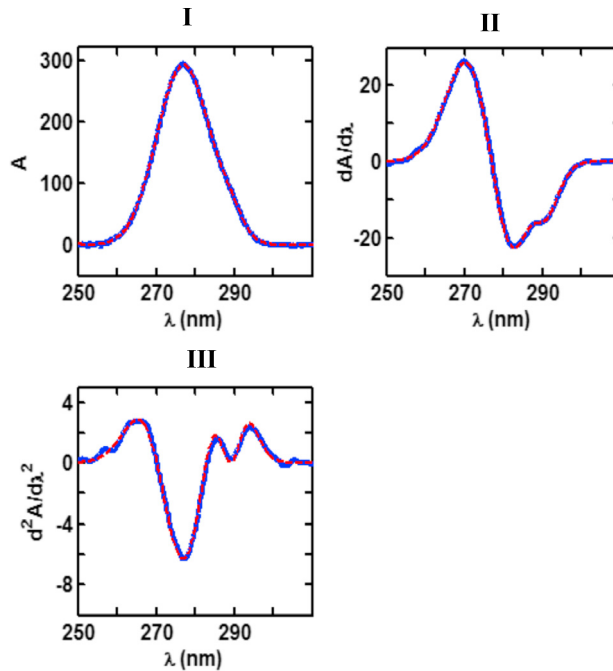

Fig. 4. Panel (I) is the plot of noisy spectral data (solid blue line) containing AWGN with SNR 40 dB. It is overlaid with estimated spectral response (red colored stippled line) using proposed scheme. Panels (II) and (III) are estimated first and second order derivative (solid blue lines) using proposed algorithm with the designed matrix based on rectangular rule. The computed true value of derivatives (red colored stippled lines) are overlaid. The sampling interval of the data set is 0.25 nm. (For interpretation of the references to color in this figure legend, the reader is referred to the web version of this article.)

rule (Eq. (2.4)) as used. On the other hand, Fig. 5 contains results of numerical experiment for same set up except that the designed matrix **A** based on trapezoidal rule (Eq. (2.6)) was used. The subplot I (for both Figs. 4 and 5) contains noise contaminated synthetically generated normal spectral data (blue colored thick solid line) overlaid with the computed smooth response from the proposed scheme. Note that the estimated response is fitted remarkably well with the noisy synthetic data. The subplots II and III (for both Figs. 4 and 5) contain the estimated first order derivative spectra with the proposed
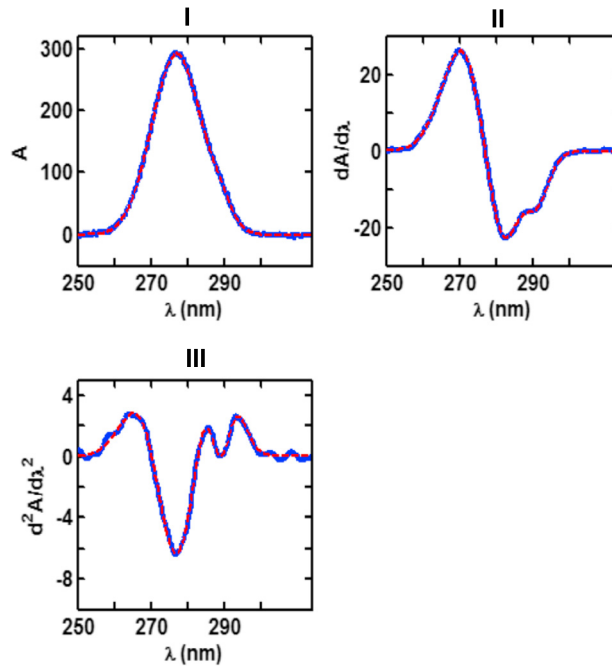
Fig. 5. Panels (I)–(III) are same as Fig. 4 except that the designed matrix used is based on trapezoidal rule. (For interpretation of the references to color in this figure, the reader is referred to the web version of this article.)

scheme (blue colored solid line) overlaid with synthetically generated first order derivative spectra (red colored stippled line) using Eq. (3.2) and the second order derivative spectra with the proposed scheme (blue colored solid line) overlaid with synthetically generated first order derivative spectra (red colored stippled line) using Eq. (3.3) respectively. With a relatively low level of noise contamination the proposed scheme corresponding to two different design matrices provides reasonably robust results, although it seems that the choice of design matrix based on rectangular rule provides marginally better results than the one based on trapezoidal rule. The condition number ($\Gamma = \lambda_{max}/\lambda_{min}$), where λ_{max} and λ_{min} are the eigenvalues of the matrix **A** based on rectangular rule is 357.14, whereas Γ of matrix **A** based on trapezoidal rule is 127,323.69. This indicates that the design matrix based on rectangular rule provides more stable computational regime compared to the one with trapezoidal rule. Interestingly, in both cases the proposed algorithm took at most 4 iterations to satisfy the stopping criteria.

Next, we increased the noise level by decreasing the SNR to 20 dB. We keep the same strategy of putting the results in the same panel with subplots as we have used for Figs. 4 and 5. Fig. 6 contains results of the numerical experiment of noisy synthetic data of SNR 20 dB, where the design matrix **A** based on rectangular rule was used, where as Fig. 7 contains experimental results of same set up except that the design matrix is based on trapezoidal rule. Results clearly demonstrate that the choice of system matrix based on rectangular rule is preferable to that of trapezoidal rule especially when the data interval Δ is substantially low and the data contain moderately high white Gaussian noise. The results as shown in Figs. 4, 5, 6 and 7 clearly demonstrate following characteristics:

1. In the computed normal spectral response the dominant component (even without noise) masks the other one entirely. Such situation is not uncommon in a real world scenario, which prompts for derivative spectra to achieve enhanced resolution,
2. The proposed algorithm is able to retrieve first and second order derivative spectra fairly robust, although second order derivative spectra seems to be less robust compared to the first order derivative spectra.
3. The proposed algorithm demonstrates a high level of robustness even when noise level is high.

The conventional Fourier transform and the difference scheme in estimating derivative spectra (both first and second order) fail spectacularly even when noise level in data is comparatively mild. On the other hand, the proposed algorithm is reasonably efficient and sufficiently robust in generating both first and second order derivative spectra even when noise level is relatively high. However, it is clear that with an increased value of noise level the results progressively deteriorate with the presence of low frequency variability. This may be explained as while the proposed algorithm was filtering out the AWGN, the red noise which is an integral of white noise crept into, and as the red noise contains more energy in the low frequency range it becomes prominent with a high noise level and with a high order of derivative.
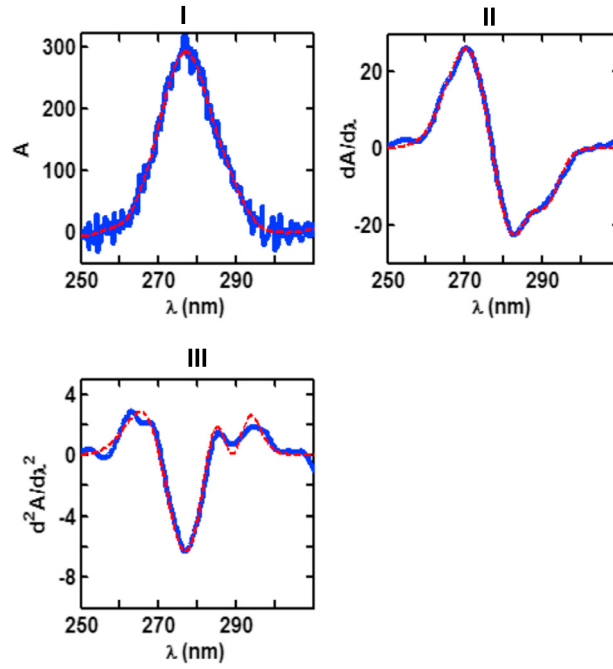
Fig. 6. Panels (I)–(III) are same as Fig. 4 except that the data contain higher level of AWGN with SNR 20 dB. (For interpretation of the colors in this figure, the reader is referred to the web version of this article.)
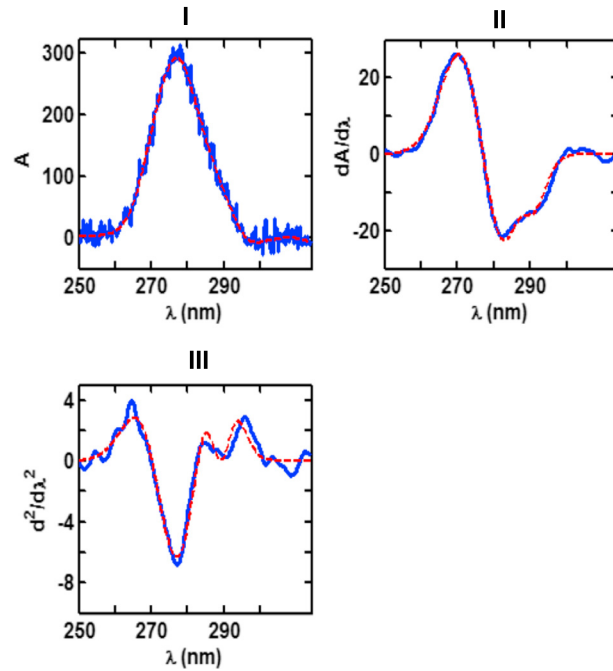

Fig. 7. Panels (I)–(III) are same as Fig. 5, except that data contain higher level of AWGN with SNR 20 dB. (For interpretation of the colors in this figure, the reader is referred to the web version of this article.)

3.2. Spectral data on water

We applied our algorithm on the published absorbance and reflectance spectral data in visible to near infrared range both for fresh water and coastal water conditions. Our choice has a special significance in the context of environmental assessment either directly by spectroscopic measurements from the collected samples or through airborne based remote sensing technique. The hyperspectral imaging which is a widely used remote sensing technique uses a wide spectral range from
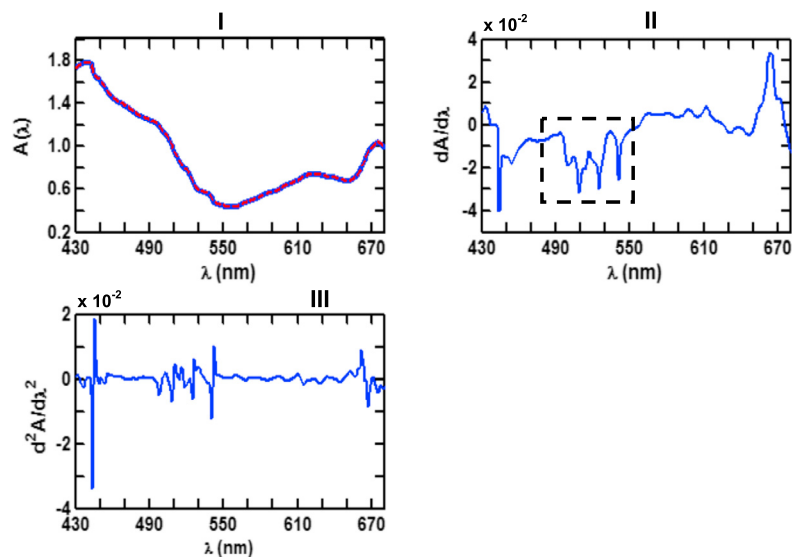
Fig. 8. Panel (I) is the plot of average absorbance spectral data (solid blue line) over Lake Taihu. The data is obtained by digitizing Fig. 5 of [33] and then it is resampled and replotted. The red colored stippled line is the estimated absorbance spectra using the proposed algorithm. Panels (II) and (III) are estimated first and second order derivative spectra. The inscribed rectangle (black colored stippled line) in the panel (II) denotes the region is zoomed and is presented later. (For interpretation of the references to color in this figure legend, the reader is referred to the web version of this article.)

ultra violet-visual to infrared. Differentiating the spectral mixture in order to estimate subpixel abundance of target species in a medium is an important exercise where derivative spectroscopy has a major role [32]. We select two examples where spectral absorbance and reflectance data were obtained (from published literature) in studying chlorophyll-a (Chl-a) concentration in fresh water and seawater respectively. The spectral range considered for both examples lies between 430–680 nm. We digitized the published data, compiled and reprocessed, and then used those in our studies. The raw digitized data was a set of discrete values which are unevenly spaced. We piecewise interpolate the discrete data set with Hermite interpolation and then resampled the interpolated data with a sampling interval 1 nm. The resampled data interval is consistent with the original data as reported in the literature. We discuss about experimental results in the following:

3.2.1. Absorbance spectra on fresh water

We consider experimental data of spectral absorbance in the visible range for Lake Taihu in China. The spectral response due to algal bloom at Lake Taihu, a fresh water lake is studied in [33]. In our study we digitized a portion of Fig. 5 in [33] which describes variation of mean absorption coefficients versus spectral wavelength during summer time. The digitized normal spectral data ranging from 430 nm to 680 nm is presented in the panel (I) of Fig. 8. An extensive study is made in [33] on the growth of phytoplankton and associated Chl-a concentration in a fresh water condition. They indicated that there are two major peaks of mean absorption coefficient, one in the blue region (approximately 440 nm) and the other in the red region (approximately 675 nm) which correspond to low Chl-a specific absorptivity due to larger cell size. They also suggested possible absorption of various other photosynthetic or photoprotective pigments in the spectral ranges 400–550 and 600–650 nm. However, normal spectral response does not provide strong evidences for that. We made derivative analysis using the proposed algorithm. The first and second order derivative spectra are presented in the panels (II) and (III) of Fig. 8 respectively. Clearly, there are several peaks in both the first and second order derivative spectra. In Fig. 9 we present the zoomed portion (inscribed rectangle with stippled line) of Fig. 8. Several peaks (marked with A, B, C and D) are clearly depicted within the range from 490 to 540 nm.

3.2.2. Reflectance spectra on sea water

We next consider the published reflectance spectral data from hyperspectral imaging over Azov Sea [34] in conducting numerical experiment with the proposed scheme. We digitized reflectance spectral profile (their Fig. 7) and selected the spectral range from 430 to 680 nm. This would give us the opportunity to compare absorption and reflectance spectral properties of phytoplankton at two different media (fresh water and salt water), although in this paper we are not focusing on the detailed studies of spectral properties of phytoplankton. The digitized and resampled reflectance spectral data are presented in panel (I) of Fig. 10. An inverse correlation between absorbance and reflectance spectra in the 430–680 nm range is clearly apparent, although the ambient media are different. There are minor peaks and shoulders in the normal spectra which are not very distinct all along the profile. We conducted derivative analysis using the proposed algorithm. The first and second order derivative spectra are presented in the panels (II) and (III) of Fig. 10 respectively. The derivative spectra reveal several characteristic peaks which are not very conspicuous in the normal reflectance spectra. In Fig. 11 we present the zoomed portion (inscribed rectangle with stippled line) of Fig. 9. Several peaks (marked with A, B, C, D, E, F
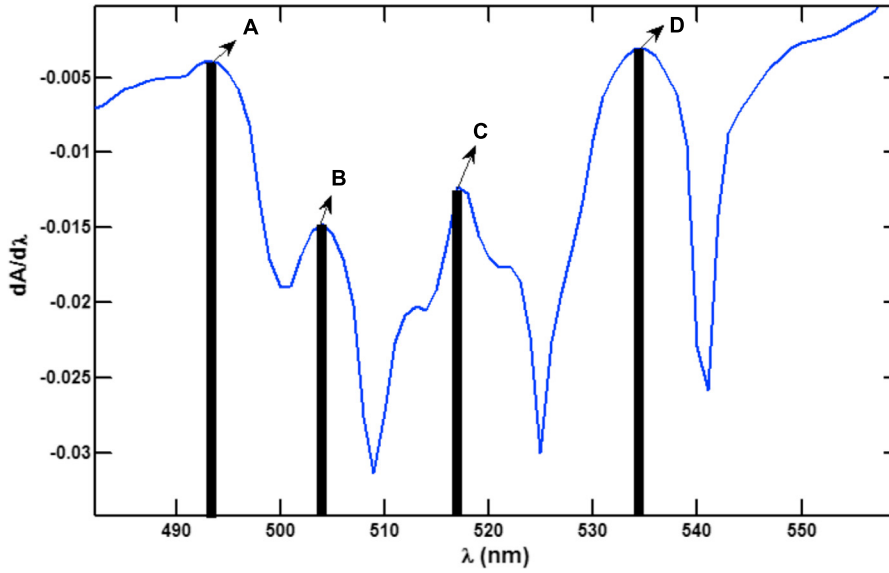
Fig. 9. Plot of the first order derivative spectra of the zoomed portion in the panel (II) of Fig. 8. (For interpretation of the colors in this figure, the reader is referred to the web version of this article.)
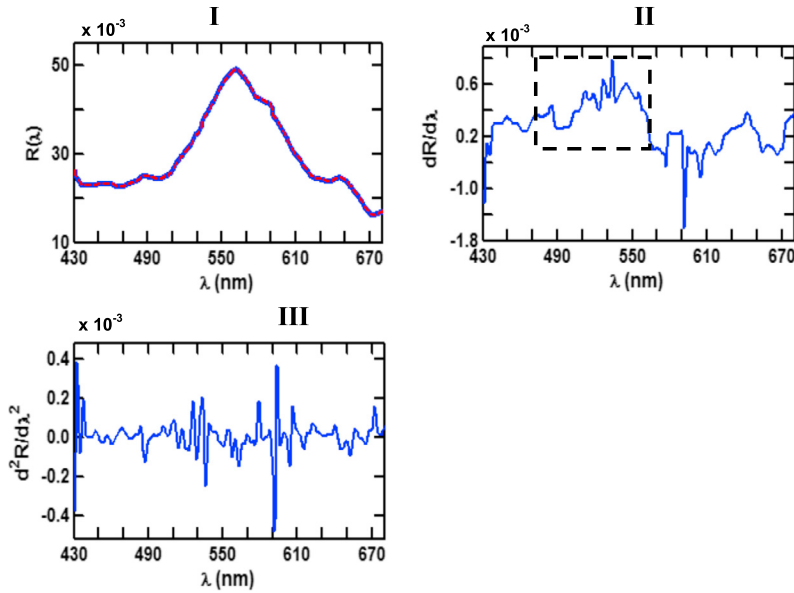

Fig. 10. Panel (I) is the plot of reflectance spectra (solid blue line) over Azov Sea. The data is obtained by digitizing Fig. 7 of [34] and then it is resampled and replotted. The red colored stippled line is the estimated reflectance spectra using the proposed algorithm. Panels (II) and (III) are estimated first and second order derivative spectra. The inscribed rectangle (black colored stippled line) in the panel (II) denotes the region is zoomed and is presented later. (For interpretation of the references to color in this figure legend, the reader is referred to the web version of this article.)

and G) are clearly depicted within the range from 480 to 570 nm. Those peaks possibly correspond to the *endmembers* of the spectral mixture.

4. Conclusion

A robust and efficient algorithm of estimating first and second order derivative spectra are developed. The algorithm is based on the framework of an inverse problem. The numerical experiments were carried out on synthetic data with varied level of additive white Gaussian noise. It is observed that two popularly used direct methods, such as Fourier transform based method and the central difference scheme provide acceptable results only when the data are noise free and sufficiently smooth. The direct methods fail spectacularly when the data contain even a mild level of noise. On the other hand,
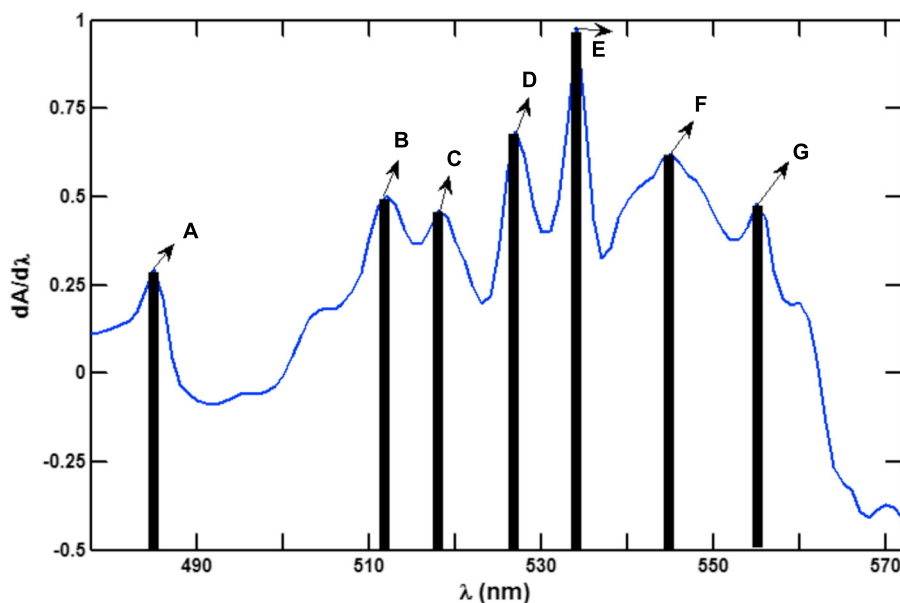
Fig. 11. Plot of the first order derivative spectra of the zoomed portion in the panel (II) of Fig. 10. (For interpretation of the colors in this figure, the reader is referred to the web version of this article.)

the proposed algorithm clearly demonstrates sufficient robustness in both first and second order derivative estimation from normal spectra. It is also observed that the derivative estimation is principal in differentiating the spectral mixing to identify the *endmembers* which are otherwise masked within the spectral response of dominant component. The algorithm is also used successfully in estimating first and second order derivative of normal absorbance and reflectance spectra in the visible range to study phytoplankton or dissolved organic matters in fresh water and coastal water conditions.

References

[1] V.J. Hammond, W.C. Price, A new system for the elimination of scattered light effects in spectrophotometers, J. Opt. Soc. Am. 43 (1953) 924.
[2] C.S. French, A.B. Church, R.W.A. Eppley, A derivative spectrophotometer, Carnegie I Wash 53 (1954) 182–184.
[3] F. Singleton, G.L. Collier, Infra-red analysis by the derivative method, J. Appl. Chem. 6 (1956) 495–510.
[4] A.E. Martin, Difference and derivative spectra, Nature 180 (1957) 231–233.
[5] J.K. Kaupinen, D.J. Moffatt, H.H. Mantsch, D.G. Cameron, Fourier self deconvolution: a method for resolving intrinsically overlapped bands, Appl. Spectrosc. 35 (1981) 271–276.
[6] P.R. Griffiths, Fourier transform infrared spectrometry, Science 222 (1983) 297–302.
[7] G. Talsky, Spectrophotometry, Law and High Orders, VCH, Verlaggesellsch, GmbH, Weinheim, 1994.
[8] K. Ahnert, M. Abel, Numerical differentiation of experimental data: local versus global methods, Comput. Phys. Commun. 177 (2007) 764–774.
[9] A. Savitzky, M.J.E. Golay, Smoothing and differentiation of data by simplified least squares procedures, Anal. Chem. 36 (1964) 1627–1639.
[10] P.A. Gorry, General least squares smoothing and differentiation by the convolution (Savitzky–Golay) method, Anal. Chem. 63 (1990) 570–573.
[11] C.H. Reinsch, Smoothing by spline functions, Numer. Math. 16 (1971) 451–454.
[12] W.H. Press, S.A. Teukolsky, W.T. Vetterling, B.P. Flannery, Numerical Recipes in Fortran: The Art of Scientific Computing, Cambridge University Press, 1992.
[13] T. Wei, Y.C. Hon, Y.B. Wang, Reconstruction of numerical derivatives from scattered noisy data, Inverse Probl. 21 (2005) 171–179.
[14] S. Ahn, U. Jin Choi, A.G. Ramm, A scheme for stable numerical differentiation, J. Comput. Appl. Math. 186 (2006) 325–334.
[15] Y. Leong Yeow, Y.K. Leong, A general computational method for converting normal spectra into derivative spectra, Appl. Spectrosc. 59 (2005) 584–592.
[16] R. Chartrand, Numerical differentiation of noisy, nonsmooth data, ISRN Appl. Math. 164564 (2011).
[17] E. Kreyszig, Advanced Engineering Mathematics, 8th ed., John Willey & Sons, New York, 1999.
[18] A.N. Tikhonov, V.Y. Arsenin, Solutions of Ill-Posed Problems, John Willey & Sons, New York, 1977.
[19] P.C. Hansen, Analysis of discrete ill-posed problems by means of the L-curve, SIAM Rev. 34 (1992) 561–580.
[20] K. Ito, B. Jin, T. Takeuchi, A regularization parameter for nonsmooth Tikhonov regularization, SIAM J. Sci. Comput. 33 (2011) 1415–1438.
[21] K. Ito, B. Jin, T. Takeuchi, Multi-parameter Tikhonov regularization – an augmented approach, arXiv:1306.5984v1, 2013.
[22] T. Regińska, A regularization parameter in discrete ill-posed problems, SIAM J. Sci. Comput. 17 (1996) 740–749.
[23] I.G. Roy, On robust estimation of discrete Hilbert transform of noisy data, Geophysics 78 (2013) V239–V249.
[24] I.G. Roy, On computing the gradients of potential field data in space domain, J. Geophys. Eng. 10 (2013) 035007.
[25] G. Wahba, Spline Models for Observational Data, SIAM, Philadelphia, 1990.

[26] V.A. Morozov, Regularization Methods for Ill-Posed Problems, CRC Press, Florida, 1993.
[27] H.W. Engl, On the choice of the regularization parameter for iterated Tikhonov regularization of ill-posed problems, J. Optim. Theory Appl. 52 (1987) 209–215.
[28] I.G. Roy, A robust descent type algorithm for geophysical inversion through adaptive regularization scheme, J. Appl. Math. Model. 26 (2002) 619–634.
[29] I.G. Roy, Iteratively adaptive regularization in inverse modeling with Bayesian outlook – application on geophysical data, Inverse Probl. Sci. Eng. 13 (2005) 655–670.
[30] K. Ito, B. Jin, A new approach to nonlinear constrained Tikhonov regularization, Inverse Probl. 27 (2011) 105005.
[31] R. Lange, J. Frank, J.-L. Saldana, C. Balny, Fourth derivative UV-spectroscopy of proteins under high pressure I. Factors affecting the fourth derivative spectrum of the aromatic amino acid, Eur. Biophys. J. 24 (1996) 277–283.
[32] J. Zhang, Derivative spectral unmixing of hyperspectral data applied to mixtures of lichen and rock, IEEE Trans. Geosci. Remote Sens. 42 (2004) 1934–1940.
[33] Y. Zhang, Y. Yin, M. Wang, X. Liu, Effect of phytoplankton community composition and cell size on absorption properties in eutrophic shallow lakes: field and experimental evidence, Opt. Express 20 (2012) 11882–11898.
[34] A.A. Gitelson, B.C. Gao, R.R. Li, S. Berdnikov, V. Saprygin, Estimation of chlorophyll-a concentration in productive turbid waters using a hyperspectral imager for the coastal ocean – the Azov sea case study, Environ. Res. Lett. 6 (2011) 024023.
[35] J. Cullum, Numerical differentiation and regularization, SIAM J. Numer. Anal. 8 (1971) 254–265.
[36] S. Lu, S.V. Pereverzev, Numerical differentiation from view point of regularization theory, Math. Comput. 75 (2006) 1853–1870.
[37] A.G. Ramm, A.B. Smirnova, On stable numerical differentiation, Math. Comput. 70 (2001) 1131–1153.
[38] B. Hofmann, Approximate source conditions in Tikhonov–Phillips regularization and consequences for inverse problems with multiplication operators, Math. Methods Appl. Sci. 29 (2006) 351–371.